James T. Baylot
Waterways Experiment Station
Vicksburg, MS 39180-6199

Fully Coupled FE Analyses of Buried Structures

Current procedures for determining the response of buried structures to the effects of the detonation of buried high explosives recommend decoupling the free-field stress analysis from the structure response analysis. A fully coupled (explosive–soil structure) finite element analysis procedure was developed so that the accuracies of current decoupling procedures could be evaluated. Comparisons of the results of analyses performed using this procedure with scale-model experiments indicate that this finite element procedure can be used to effectively evaluate the accuracies of the methods currently being used to decouple the free-field stress analysis from the structure response analysis. © *1994 John Wiley & Sons, Inc.*

INTRODUCTION

Procedures for designing buried structures to resist the effects of the detonation of buried high explosives decouple the structure response analysis from the determination of the free-field stresses (those stresses that would be present at the structure location if the structure were absent). The procedure recommended in TM5-855-1 (U.S. Army, 1986) accounts for reflection of the stress wave as it reaches the structure and relief of the reflected wave by the free surface on the back of the wall. This procedure is based on empirical data that show that typically the peak stress (load) applied to the structure is 1.5 times the peak free-field stress and the structure load decays to the free-field stress in a time equal to 12 transit times of a stress wave through the thickness of the wall slab. The structure-medium-interaction (SMI) method recommended by Drake et al. (1987) and Weidlinger and Hinman (1990) uses linear-elastic plane-wave theory to determine the structure loads based on the free-field stresses and velocities and the structure velocity. The interface stress, σ_i, applied to the structure, is given by

$$\sigma_i = \sigma_{ff} + \rho c(V_{ff} - V_s) \tag{1}$$

where σ_{ff} is the free-field stress, ρc is the acoustic impedance of the soil, V_{ff} is the free-field particle velocity, and V_s is the structure velocity. Tension at the soil–structure interface is not possible; therefore:

$$\sigma_i \geq 0.0. \tag{2}$$

The TM5-855-1 and SMI method were evaluated against test data by Baylot and Hayes (1989). It was found that the TM5-855-1 method significantly overpredicted loads on structures. Based on experimental data (Hayes, 1989), the load at the center of the structure rises quickly to a peak value and then drops back to a much lower value (sometimes 0). The SMI method significantly underpredicts the postpeak loads and this underprediction leads to an underprediction of structural response.

Clearly, a better method of predicting the postpeak loads is needed. Free-field stress and velocity and structure load and response data have been collected (Hayes, 1989) to study soil–structure interaction (SSI). It is difficult to evalu-

Received February 21, 1994; Accepted April 11, 1994.
Shock and Vibration, Vol. 1, No. 5, pp. 451–460 (1994)

CCC 1070-9622/94/050451-10

ate SSI using these data because there are not enough data to define the stress and velocity distributions in the free-field and at the soil–structure interface. Minor variations in gage response also make interpretation of these data difficult. Analyses, verified by comparison with experimental results, are needed to study SSI.

An analysis procedure for studying SSI was developed and this procedure was used to analyze two scale-model experiments (Hayes, 1989). Comparisons between the analysis results and experimental data were made to verify that the analysis procedure captured the important characteristics of SSI. These comparisons are presented in this article.

TEST 1

A cross section through the test bed for these two tests is given in Fig. 1. Details of the experiments are provided in Hayes (1989) and Baylot (1993). The test structure consisted of a reaction structure and a test element (wall slab). The reaction structure was a box structure with one side missing. The test element was bolted onto the open side of the reaction structure to form the last wall of the test structure. Active instrumentation for these tests included accelerometers and stress gages placed in the soil, gages to measure normal stress at the soil–structure interface, and accelerometers to monitor structure motion. A passive gage was used to record maximum and residual deformation of the wall slab. The procedure for conducting test 1 was: excavate the test pit (controlled backfill area); place controlled backfill up to the elevation of the floor slab; place the reaction structure of the test pit; bolt that test element to the reaction structure; complete placement of the backfill; place the explosives; and conduct the experiment. Free-field gages were placed at the appropriate stage of backfill placement. The backfill material was a nearly saturated clay with a very low shear strength.

The test element for test 1 was 110-mm thick and the principal steel ratio was 0.01. The steel ratio is the area of a reinforcing bar divided by the effective depth of the wall and the spacing between adjacent bars. The same amount of steel was placed near each face of the wall slab.

TEST 2

The same procedure used to conduct test 1 was used to conduct test 2, except for the placement of the reaction structure, which was already in place. In test 2, the wall was 220-mm thick and the principal steel ratio was 0.005. Other test details were essentially the same as for test 1.

ANALYSIS REQUIREMENTS

An analysis that includes both the structure and the soil in front of it is needed to study the interaction of the soil with the structure. This analysis is often accomplished by using the "soil island" method. The structure and a portion of the surrounding soil are modeled (Fig. 2). In this model, the appropriate boundary conditions must be applied to the soil island boundaries so that the

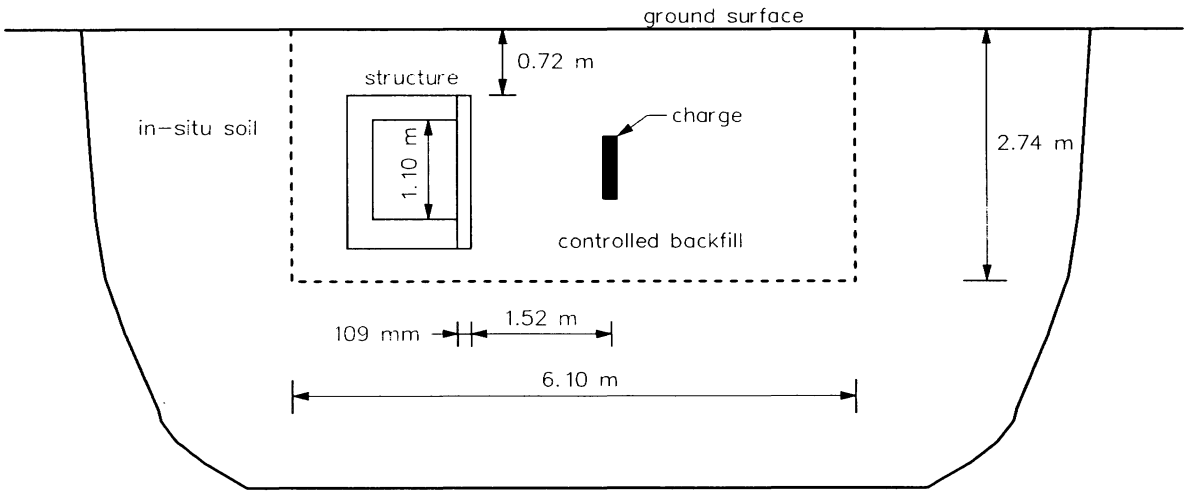

FIGURE 1 Test geometry.

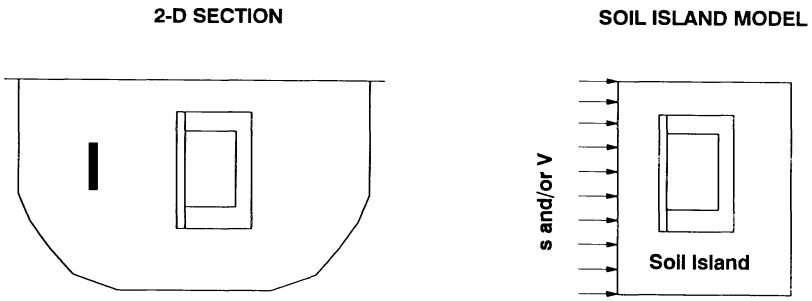

FIGURE 2 Soil island model.

model behaves as if all of the soil were modeled. The left boundary of this figure is particularly important because the velocities and/or stresses input on this boundary represent the primary effects of the detonation of the explosive. Typically the stresses and/or velocities applied to this boundary are determined by a separate analysis that does not include the structure. In order to avoid including the detonation of the weapon in the analysis, the left boundary must be placed between the charge location and the structure. Because the explosive in the test is close to the structure, the boundary must be placed even closer to the structure.

Soil island analyses are valid up to the time when the soil island boundary affects the solution. On the side of the explosive, the stresses and velocities at the location of the boundary are affected by the structure. These effects are not included in the stresses and/or velocities which were input on the boundary. The valid simulation time is the total travel time from the soil island boundary to the structure, back to the boundary, and then back to the structure again. Because of the closeness of the charge to the structure, the soil island method can only be used to study the very early loads on the structure. Therefore, the soil island method is not appropriate for studying late-time SSI.

Because a boundary cannot be introduced between the explosive and the structure, the analysis method must be capable of modeling the detonation of the explosive, propagation of stresses through the soil, interaction of the soil with the structure, and large deformation response of the structure. The explicit finite-element (FE) method is capable of meeting all of these requirements. The FE computer code, DYNA3D (Hallquist and Benson, 1982), includes the Jones–Wilkens–Lee (JWL) equation of state to model the detonation of the explosive. The Cap model (Sandler and Rubin, 1979; Simo et al., 1988) can be used to model the soil. A sliding interface capable of allowing sliding with friction, as well as debonding and rebonding of the soil and structure, is available. Constitutive models for concrete are also available. DYNA3D contains the methodology needed to perform these analyses; therefore, it was selected for these analyses.

Several problems were encountered in attempting to perform these analyses. These problems, the solutions to these problems, and verification of the improved computer code have been published (Baylot, 1993). The version of the Cap model that existed in DYNA3D could not converge to a solution for the properties of the soil used in these experiments. Pelessone experienced similar problems and developed a Cap model that overcame these problems. This new Cap model was developed by General Atomics, Inc., for the Defense Nuclear Agency. Details of the model were presented by Schwer and Murray (1994). This Cap model was installed in DYNA3D. In the new Cap model (as well as the old one) the bulk modulus is constant. A constant bulk modulus is adequate for most situations, but is not adequate for modeling soil over the wide range of pressures required to model the soil from the explosive out to the structure. The Cap model was modified to provide a bulk modulus that varies with pressure.

Stable solutions for explosive detonation and ground shock propagation could not be obtained using the default values of the artificial viscosity coefficients. Increasing the values of the coefficients stabilized the solution, but also significantly increased the rise time to peak stress. In DYNA3D, linear and quadratic artificial viscosity forces are used to stabilize the solution. The magnitude of the force is a function of the volumetric strain rate, the viscosity coefficients, and

the characteristic length of the element. The characteristic length of the element is taken as the cube root of the element volume. This is appropriate for relatively uniform grids. Because of the cylindrical grid used to model the explosive and the soil near it and the rapid decrease in stresses as the shock propagates away from the center, it is more appropriate to use the radial dimension of the element for the characteristic length. Using the cube root of the volume for the characteristic length results in low artificial viscosity forces near the center of the grid. The low forces can be offset by using higher values for the artificial viscosity coefficients; however, at distances farther away from the charge, the artificial viscosity forces will be too high. It was determined that stable solutions could be obtained without artificially increasing rise times by using artificial viscosity coefficients that decrease with increasing distance from the explosive. This method simulates the effect of using the radial dimension of the element for its characteristic length.

Parametric analyses (Baylot, 1993) were performed to determine the optimum grid size and other parameters such as artificial viscosity coefficients, and the critical time step. These analyses showed that the radial dimension of the element should be approximately 2.5 cm to adequately model the rise time to peak stress at the structure location.

Nonreflecting boundaries, which function adequately in the nonlinear response region, are required to reduce the area of soil that must be modeled in order to make the solution of the problem feasible. The existing nonreflecting boundary, when used with the Cap model, behaved more like a rigid boundary than a nonreflecting boundary because the nonreflecting boundary subroutine used the elastic properties of the soil. The elastic stress–strain behavior of the soil is much stiffer than the actual behavior of the soil. The nonreflecting boundary was modified to use shear and bulk moduli which are softer than the elastic constants. The modified boundary was verified by performing analyses with the boundary and comparing these results to results from analyses in which the boundary was far away. Verification of the modifications to the code and comparisons to free-field stress and velocity data have been published (Baylot, 1993). The structure was added to the analyses so that the analyses now include the explosive, the soil, and the structure.

PURPOSE OF ANALYSES

The purpose of these analyses is to study details of SSI, not necessarily to perform the most accurate analysis possible. The purpose of these analyses is not to develop methods of predicting free-field stress or structure response. The purpose of the comparisons presented in this article is to verify that the correct SSI phenomena are being modeled. The structure (Fig. 1) in the experiment was a shallow-buried structure and the soil–air interface had some effect on the loads on and response of the structure. The presence of a water table below the structure may also have had an effect. These effects were not included in the analysis because they further complicate the study of SSI. The analysis was further simplified by using a two-dimensional (2-D) model. The 2-D model also allows the use of a finer grid spacing so that very short rise times can be modeled. Analyses were performed (Baylot, 1993) to demonstrate that meaningful results could be obtained using a 2-D model. Parametric analyses were performed to determine the charge size needed to match the free-field stress and velocity histories measured for the location of the center of the wall of the test element.

ANALYSIS MODEL

The model used to analyze these experiments is outlined in Fig. 3. Because the free surface and water table were neglected, the model is symmetric with respect to the structure midheight and only half of the structure is modeled. Slide surfaces, which allow sliding with friction and separation and recontacting between opposing surfaces, were used between the soil and structure. Because the soil had a very low shear strength the coefficient of friction was set equal to zero. The slide surface below the structure was extended into the soil so that the soil in front of the structure could flow past the structure. The grid to the left of the charge was included so that the free-field stresses and velocities could be determined in the same analysis as the structure response. This procedure for computing the free-field stresses is similar to the method used to collect the data in the experiment.

The grid used to model the structure is shown in Fig. 4. Reinforcement was modeled by overlaying a grid of truss elements on the solid element grid used to model the concrete. The con-

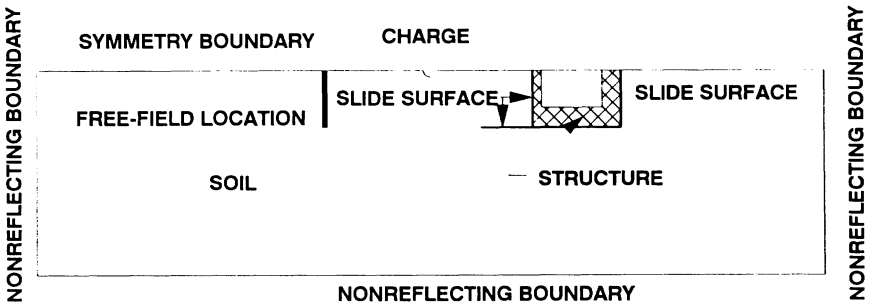

FIGURE 3 Grid outline.

crete was modeled using the concrete/geologic material model with the parameters recommended by Moor and summarized by Whirley and Engelmann (1992). The unconfined compressive strength, f'_c, of the concrete was 41 MPa and Poisson's ratio was 0.23. The principal steel was modeled as an elastic–perfectly plastic material with a yield strength of 610 MPa, a modulus of elasticity of 207,000 MPa, and a Poisson's ratio of 0.3. The concrete and steel strengths were increased by 20% to account for strain-rate effects. Yield-line analyses for a uniform load indicated that the predicted capacity of the wall slab is approximately 10% higher if the slab is analyzed as a two-way slab. The strengths of the concrete and steel were increased by 10% to account for the two-way action of the slab not modeled in the FE analysis. The elastic modulus of the steel was also increased by 10% because the two-way action also increases the elastic stiffness of the slab.

Shear stirrups in the slab were modeled as truss elements. These shear stirrups were horizontal bars connecting the inner and outer layers of vertical wall steel in the test element. In the initial analyses of test 1, the shear deformation of the slab was overpredicted. There are two possible explanations for the overprediction of shear response: the stirrups in the experiment are more effective in controlling the shear response of the slab than the stirrups modeled in the analysis, and the FE model of the concrete is too soft in shear. The diagonal bars shown in Fig. 5 were added to make the response mode in the analyses more nearly match the experiment. This change satisfied the purpose for these analyses, but this issue should be investigated further in the future so that the modeling of the shear response of concrete can be improved. The model of the rod used to connect the test article to the reaction structure is also shown in Fig. 5. More details on the determination of material properties and the development of the model are available (Baylot, 1993).

COMPARISON WITH TEST 1

The computed and measured free-field horizontal stresses at the location of the center of the wall are compared in Fig. 6. The computed history was shifted in time to match the arrival time of

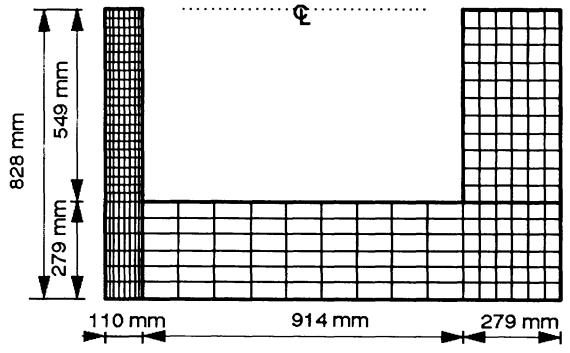

FIGURE 4 Grid for structure.

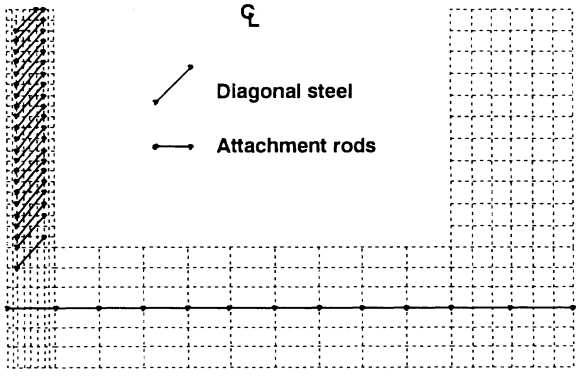

FIGURE 5 Diagonal steel.

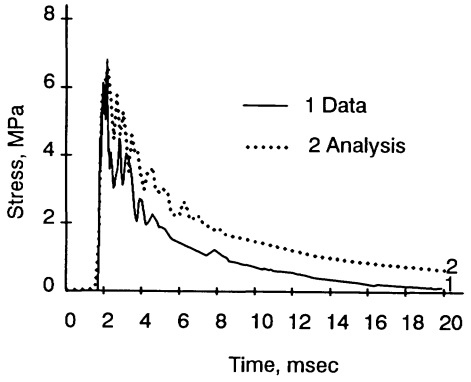

FIGURE 6 Free-field stresses.

the measured history. All other histories for this test were shifted by this amount. The computed peak stress matched the data very well, and the characteristics of the computed history match the characteristics of the measured history. The late-time computed stresses are significantly higher than those measured in the experiment. This overprediction is due in part to the free surface (Fig. 1), which was not modeled in the experiment.

TM5-855-1 (U.S. Army, 1986) provides equations for computing the stress history at a point, *P*. These equations do not allow for the presence of a free surface. The manual does, however, provide a method for accounting for the free surface. When the stress wave propagating away from the explosive source reaches a point on the surface, a tensile wave begins to propagate back into the soil. This interaction occurs all along the soil–air interface and the tensile waves propagate toward point *P*. The stress history at point *P* is the combination of these tensile waves with the shock wave propagating to point *P* directly from the source. The TM5-855-1 method for accounting for the free surface is as follows: compute the free-field stress at point *P*; compute the free field stress at point *P* caused by the detonation of the explosive located at an image point, *I*; and subtract the image point history from the free-field stress history at point *P*. The image source is placed at a range, *R*, from point *P*, where *R* is the shortest distance from the source to the free surface and then to the target point, *P*.

Free-field stress data are compared with three different predictions of the free-field stress in Fig. 7. The effect of the free surface is neglected in one of these curves (uncorrected prediction). One of these predictions (corrected prediction) is based on the TM5-855-1 method of including the effect of the free surface. The predicted free surface effects arrive too late (approximately 6.5 ms). This method assumes that the relief wave from the free surface travels at the loading wave velocity of the soil, and it should travel at the unloading wave velocity. If the unloading velocity was used the free surface effects would arrive at approximately 5 ms. The method also overpredicts the effect of the free surface. The predicted stresses very quickly go to 0 and then go into tension (tension not shown in figure). One method of reducing the error is predicting the free-field stress is to assume that the refraction at the surface is less than perfect. Instead of subtracting the image point free-field stress from the free-field stress at the target location, subtract some fraction of the image point free-field stress history. Another prediction was made in which half of the image point free-field stress was subtracted from the target point stress. In this new prediction the time of arrival of the image point history was shifted to allow for the propagation of the relief wave at the unloading velocity. As shown in Fig. 7, the (modified corrected) predicted free-field stress history matches the free-field data much better. These analyses demonstrate that free surface effects are the primary reason that the late-time loads are overpredicted. These analyses also indicate that a better simplified method for predicting the effect of the free surface is needed.

Computed and measured horizontal free-field velocities are compared in Fig. 8. The computed peak is somewhat higher than the data, and the computed velocities decay faster than those obtained from the experimental data. The decay portion is different (Baylot, 1993) because of the 2-D geometry used in the analysis. The arrival

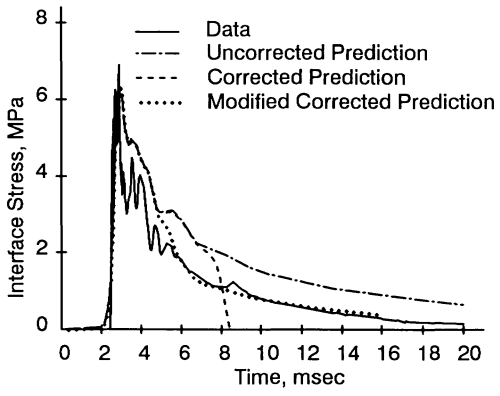

FIGURE 7 Effect of free surface.

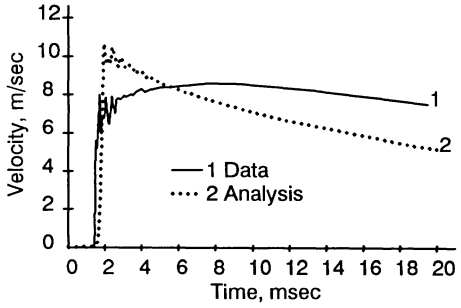

FIGURE 8 Free-field velocities.

time for velocity should be the same as the arrival time for stress. The computed arrival time for velocity should agree with the arrival time based on data because the computed velocity history was shifted by the same amount of time as the computed stress history. The stress and velocity arrival times in the analysis are the same, but those arrival times for the data are not the same. The difference in arrival times between the measured velocity and stress is one of the problems associated with attempting to use experimental data to evaluate SSI.

Horizontal velocities of a point at the center of the floor of the reaction structure are compared in Fig. 9. These curves represent the rigid-body motion of the structure. This figure indicates that the computed velocities are too high, but the character of the computed history matches that of the data extremely well. The overprediction of rigid-body velocity is expected because only a 2-D slice of the structure is analyzed. The load on the front wall is highly nonuniform, and the peak load is much higher nearest the charge. Therefore, the average load on a slice through the center of the structure is much higher than the average load on the whole front wall of the structure. The higher average load on the front pushes the structure through the soil faster and causes

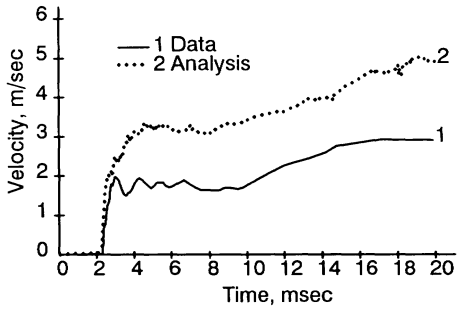

FIGURE 9 Rigid-body velocities.

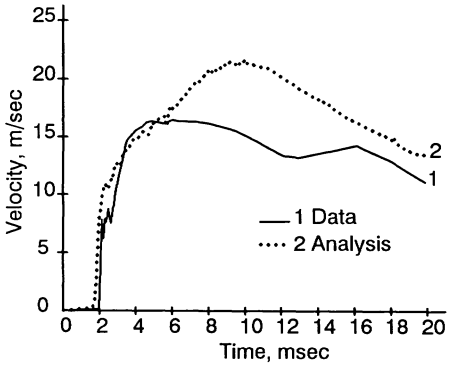

FIGURE 10 Deformational velocities.

higher loads on the back of the structure. The higher average load on the back wall causes the predicted damage to the back wall to be higher than the damage incurred in the experiment.

The velocity of the center of the wall relative to the rigid body velocity of the structure provides a measure of the rate of deformation of the wall of the structure; therefore, this relative velocity is referred to as the deformational velocity. The deformational velocity computed from the analysis is compared with that computed from the experimental data in Fig. 10. This figure shows that initially the deformational velocity was predicted very well. Later in time, the computed velocity is approximately 30% high. This overprediction is consistent with the fact that the computed late-time free-field stresses are high. Deformations computed by integrating the computed and measured deformation velocities are compared in Fig. 11. The deformation is slightly overpredicted based on comparison with the doubly integrated accelerometer record, but the peak deformation agrees extremely well with the

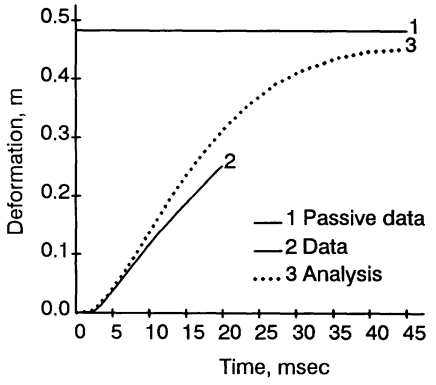

FIGURE 11 Deformation.

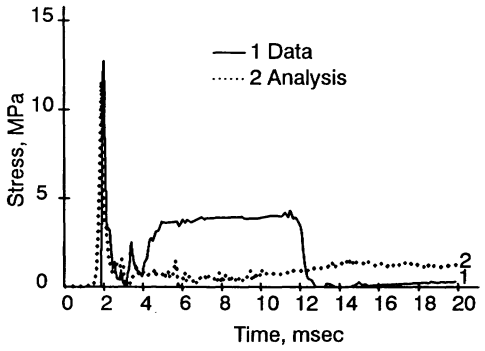

FIGURE 12 Interface stress at center.

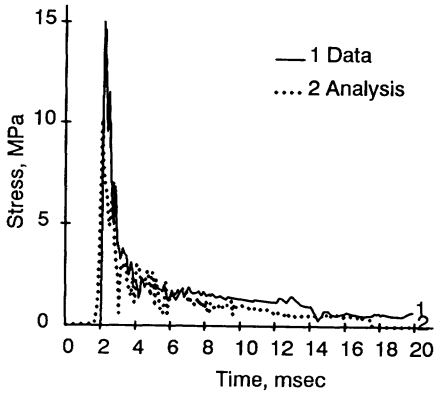

FIGURE 14 Interface stress near support.

deformation measured using a passive deformation gage.

The maximum rigid-body and deformational velocities in this experiment were approximately 3.0 and 17 m/s, respectively. The maximum rigid-body velocity determined in the analysis was approximately 5.0 m/s. Although this overprediction of rigid-body motion appears to be significant in Fig. 9, the rigid-body motion is small relative to the deformational velocity and does not significantly affect the analysis.

Computed and measured interface stresses at the center of the slab are compared in Figs. 12 and 13. Unfortunately, in this experiment, the interface stress gages near the center of the slab were squeezed by the concrete due to the large deformation that occurred in this test. This squeezing caused the hump in the data between 4 and 13 ms. Other gages in this test do indicate that there is a significant late-time load. The very early time stresses are compared in Fig. 13. The computed stress agrees very well with the measured stress. The arrival times are slightly different. The time of arrival for the interface stress gage should be the same as the time of arrival for the free-field stress gage at the same range. This is true in the analysis, but not in the experiment. Computed and measured interface stresses near the support are compared in Fig. 14. The agreement between the analysis and data is reasonably good. The measured interface stress is approximately 33% higher than the computed stress. This is partially due to the method of modeling the charge in the analysis as compared to the actual charge. In this experiment (Fig. 1), the charge is cylindrical with its axis placed vertically. In the analysis, the charge is cylindrical but is modeled in a 2-D section. This is equivalent to having the axis of the charge placed parallel to the long direction of the structure. Later in time, the low predicted interface stresses at the support may be caused by the overprediction of the rigid-body motion of the structure. The structure in the analysis is moving faster than the one in the experiment. This could cause the interface stresses to be slightly low.

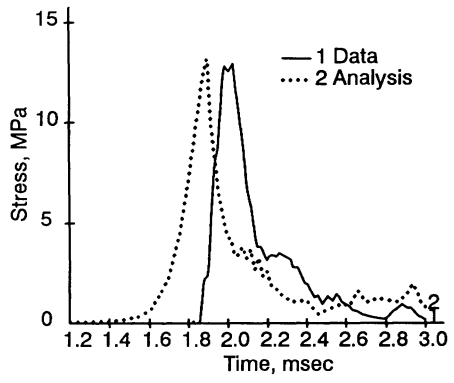

FIGURE 13 Early time interface stress near center.

COMPARISON WITH TEST 2

The same explosive charge and standoff distance used in test 1 were used in test 2. The primary difference between the two tests was the test structure. In test 2 the test slab was 220-mm thick as opposed to 110 mm in test 1. The free-field stress and velocity histories recorded for test 2 were approximately the same as those for test 1. Because the charge and standoff were the same in the analysis, the computed free-field stresses and velocity histories were identical to those in test 1. Therefore, the comparison of free-field stresses for test 2 is adequately represented by

the comparison shown for test 1 in Fig. 6. The late-time free-field stresses at the center of the structure were overestimated by approximately 0.7 MPa. The structure analysis was performed and the maximum computed deformation of the structure wall was 57 mm and the measured deformation was 38 mm. The overestimated response was due to the overestimation of the late-time free-field stresses, due to neglecting the free surface in the analysis. The goal of this study was to study SSI, not to study methods of predicting free-field stresses or methods of predicting structure response. It is important to adequately approximate the free-field stresses and structure response in order to demonstrate that the SSI is being modeled correctly. Because the free-field stress was overpredicted by approximately 0.7 MPa, the structure static capacity was increased by approximately 0.7 MPa by increasing the steel and concrete strengths by 50%, and the analysis was repeated.

The comparison of rigid-body velocities was similar to that comparison for test 1. The deformational velocities computed from the analysis compare very well (Fig. 15) with those computed from the test data. Computed and measured interface stresses at the center of the slab and near the support are compared in Figs. 16 and 17, respectively. The interface stress at the center of the slab is predicted extremely well for the entire history. Near the support, the test data show a large initial pressure spike. The magnitude of this spike is much higher than the peak pressure recorded at the center of the slab. The computed peak stress near the support is approximately the same as the computed peak stress at the center. The center of the structure is slightly closer to the explosive charge. The shock was impinges normally upon the center of the structure, but the shock wave impinges on the structure at a slight

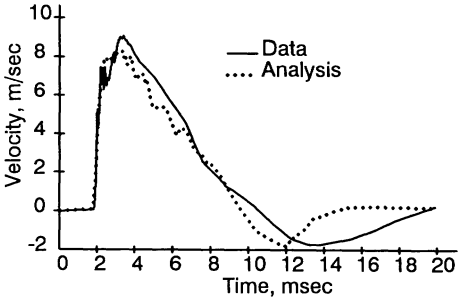

FIGURE 15 Deformational velocity, test 2.

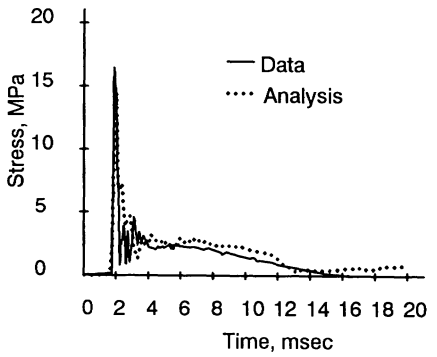

FIGURE 16 Interface stress near center, test 2.

angle near the supports. Therefore, it is reasonable to expect that the peak interface stress near the center of the slab should be higher than the peak interface stress at the support. The high pressure spike in the data may be due to the gage overregistering the stress or could be due to an inhomogeneity in the test not considered in the analysis. The prediction beyond the initial spike matches the data well.

SUMMARY

An analysis procedure, which included the detonation of the explosives, the propagation of stresses through the soil, the interaction of the soil with the structure, and the large deformation response of the structure, was needed to study SSI. This procedure was developed and 2-D plane–strain analyses were performed for comparison with two experiments conducted in wet clay. The characters of the free-field stress and velocity, and structure interface stress and velocity histories matched the experimental data

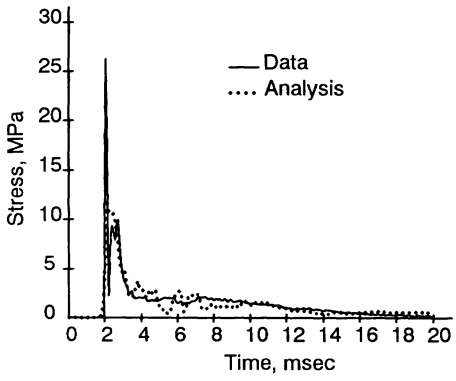

FIGURE 17 Interface stress near support, test 2.

reasonably well. In the first test, the peak values of those histories also agreed reasonably well with experimental data. In the second test, the magnitudes of the peak values matched those of the experiment once the structure's strength was enhanced to account for the overprediction of late-time free-field stresses.

CONCLUSION

The comparison of computed results with experimental results for test 1 (severe damage) and test 2 (light damage) indicates that this method (including using a 2-D geometry and neglecting the free surface and water table) of analysis captures the important characteristics of SSI. The analysis results can be used to evaluate current methods of predicting loads on buried structures and to develop new methods.

I gratefully acknowledge permission from the Chief of Engineers to publish this article.

REFERENCES

Baylot, J. T., 1993, "Loads on Structures in Low-Shear-Strength Soils Subjected to Localized Blast Effects," PhD Dissertation, University of Illinois, Champaign, IL.

Baylot, J. T., and Hayes, P. G., 1989, "Ground Shock Loads on Buried Structures," *Proceedings of the 60th Shock and Vibration Symposium,* David Taylor Research Center, Bethesda, MD, Vol. 1, pp. 331–347.

Drake, J. L., Frank, R. A., and Rochefort, M. A., 1987, "A Simplified Method for the Prediction of Ground Shock Loads on Buried Structures," *Proceedings of the 3rd International Symposium on the Interaction of Conventional Munitions with Protective Structures,* Mannheim, Germany, pp. 3–14.

Hallquist, J. O., and Benson, D. J., 1982, "DYNA3D User's Manual (Non-Linear Dynamic Analysis of Structures in Three Dimensions)," Lawrence Livermore National Laboratory Report UCID-19592, University of California, Berkeley, CA, accession number DE86010256/XAB, National Technical Information Service (NTIS), 5285 Port Royal Road, Springfield, VA.

Hayes, P. G., 1989, "Backfill Effects on Response of Buried Reinforced Concrete Slabs," U.S. Army Engineer Waterways Experiment Station Technical Report SL-89-18, Vicksburg, MS, accession number AD-A215823/6/XAB, NTIS.

Sandler, I. S., and Rubin, D., 1979, "An Algorithm and Modular Subroutine for the Cap Model," *International Journal of Numerical Analysis Methods in Geomechanics,* Vol. 3, pp. 173–186.

Schwer, L. E., and Murray, Y., 1994, "A Single Surface Three-Invariant Cap Model with Mixed Hardening," *International Journal for Numerical and Analytical Methods in Geomechanics,* to appear.

Simo, J. C., Ju, J. W., Pister, K. S., and Taylor, R. L., 1988, "An Assessment of the Cap Model: Consistent Return Algorithms and Rate Dependent Extension," *Journal of Engineering Mechanics,* Vol. 114, pp. 191–218.

U.S. Army, 1986, "Fundamentals of Protective Design for Conventional Weapons," Army Technical Manual 5-855-1, NTIS.

Weidlinger, P., and Hinman, E. E., 1990, "Cavitation in Solid Medium," *ASCE Journal of Engineering Mechanics,* Vol. 117, pp. 166–183.

Whirley, R. G., and Engelmann, B. E., 1992, "DYNA2D-A Nonlinear, Explicit, Two-Dimensional Finite Element Code for Solid Mechanics User's Manual," Lawrence Livermore National Laboratory Report UCRL-MA-110630, University of California, Berkeley, CA, accession number DE92017310/XAB, NTIS.